Sea Surface Mixed Layer during the 10–11 June 1994 California Coastally Trapped Event

C. E. DORMAN

Department of Geological Sciences, San Diego State University, San Diego, California

L. ARMI

Physical Oceanography Research Division, Scripps Institution of Oceanography, San Diego, California

J. M. BANE

Marine Sciences Program, University of North Carolina at Chapel Hill, Chapel Hill, North Carolina

D. P. ROGERS

Physical Oceanography Research Division, Scripps Institution of Oceanography, San Diego, California

(Manuscript received 12 April 1996, in final form 18 July 1997)

ABSTRACT

A midlevel, coastally trapped atmospheric event occurred along the California coast 10–11 June 1994. This feature reversed the surface wind field along the coast in a northerly phase progression. Along the central California coast, the winds at the coastal stations reverse before the corresponding coastal buoy offshore, then followed hours later by passage of the leading edge of an overcast stratus cloud. The sea surface temperature was much colder in the narrow strip along the coast. The cloud characteristics may be accounted for by a sea surface mixed layer (SSML) model beginning with the wind reversal and growing with the square root of time. Heat is lost from the SSML to the sea surface. A cloud forms when the air temperature at the top of the SSML is equal to the dewpoint. It is suggested that a bore develops on the top of the SSML, increasing the thickness of the SSML and the progression speed of the cloud to 8 m s^{-1}. There is evidence that an undular bore with a leading cloud develops in the thinner inshore SSML.

Advancing beyond Monterey Bay, horizontal density contrast is believed to have caused the bore to change character to a gravity current with a narrower cloud that passed a point inshore before the winds reversed at the buoys. The last trace of a disturbed boundary layer ended at Point Arena where strong northerly winds prevented any further northerly progression and contributed to a cyclonic eddy that was formed in the lee of the point.

Caution is suggested in the interpretation of stratus cloud phase progression without coastal wind measurements.

1. Introduction

The major characteristic of the California coastal summer atmosphere is a strong, low subsidence inversion capping a moist, cool marine layer (Neiburger et al. 1961). Over the past decade, an interest has developed in coastally trapped events on this inversion [initially Dorman (1985), (1987), (1988); Mass and Albright (1987), (1988); reviewed in Reason (1989); Reason and Steyn (1990), (1992); and others]. A coastally trapped event is defined as an elevated or depressed dense boundary layer extending more than a few hundred kilometers along the coast with a timescale of 2–3 days. As rotation is important, the event moves forward with the coast on the right. Only elevated boundary layer cases have been identified along California.

The descriptive work instigated theoretical investigations and modeling (Rogerson and Samelson 1995; Eddington et al. 1992; Skamarock et al. 1996). Some of the results have been adapted to applied forecasting (Felsch and Whitlach 1993). Due to a lack of operational mesoscale data along the coast, satellite cloud observations have been key to the recognition and estimation of the character of a northward-propagating, coastally trapped event.

This was true of the event 10–11 June 1994 when a coastal stratus overcast expanded from Point Conception to Point Arena, California. Fortunately, an unusual array of radar profilers and automated coastal meteorological

Corresponding author address: Dr. Clive E. Dorman, Dept. of Geological Sciences, San Diego State University, 5500 Campanile Drive, San Diego, CA 92182-0337.

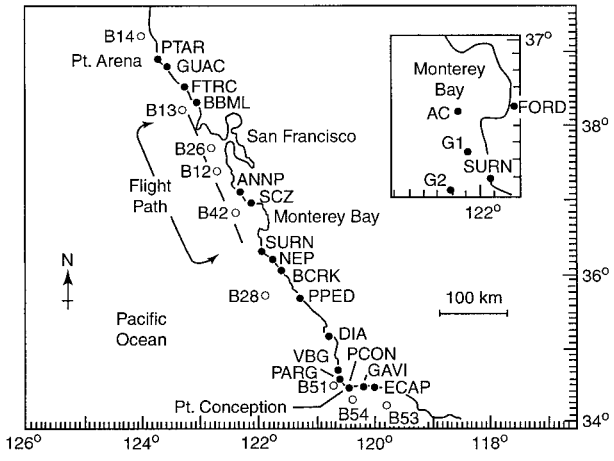

FIG. 1. Station locations.

stations were in place along the California coast at that time. A general description of this event is reported in a companion paper (Ralph et al. 1995; Ralph et al. 1998). The object of this paper is to describe the sea surface mixed layer (SSML) that contained the stratus overcast and investigate the dynamics of this layer. It will be shown that, in this case, the stratus cloud pattern was not representative of the larger, trapped progressive event and had different dynamics. The case will be made that a shallow internal boundary layer grew in the southerly winds, and processes within the SSML caused the stratus to form.

2. Observational systems

Data from 5 out of a total of the 13 Scripps Institution of Oceanography (SIO) automated meteorological stations in Fig. 1 are used in this paper (Table 1). These are low, coastal stations with anemometers on a 10-m mast. Air temperature and humidity sensors in a Gill-aspirated radiation shield and a pressure sensor are also mounted on the mast. The wind sensor was inoperable at GUAC. All SIO sensors were sampled at 1-min intervals. The Bodega Bay Marine Laboratory station made 5-min averages of winds, pressure, and humidity, and offshore measurements were taken at National Data Buoy Center buoys. These were hourly spot measurements of winds, pressure, and air and sea temperatures (Hamilton 1980). Also available are hourly measurements at the coastal CMAN station at Point Arena. Coastal observations in the Southern California Bight were obtained from the Santa Barbara Air Pollution Control District.

Radar profiler measurements were made at several coastal locations. Bill Neff at NOAA's Wave Propagation Laboratory at Boulder had profilers at Fort Bragg and Santa Cruz (SCZ), the Naval Postgraduate School had a profiler at Fort Ord (FORD), and the USAF maintained three profilers at Vandenberg AFB (VBG). An acoustical sounder was operated at the Diablo Canyon Power Plant (DIA) by Pacific Gas and Electric Company.

An instrumented light aircraft was flown over the coastal area on 10 and 11 June (Bane et al. 1995). The

TABLE 1. Station data: NDBC—National Data Buoy Center; NPGS—Naval Post Graduate School; WPL—Wave Propagation Lab, Boulder, Colorado; SIO—Scripps Institution of Oceanography; SBAPC—Santa Barbara Air Pollution Control District; UC—University of California.

Designation	Position	Height (m)	Type	Operator	Area name
B14	39.2°N, 124.0°W	0	Buoy	NDBC	
PTAR	39.0°N, 123.7°W	12	CMAN	NDBC	Pt. Arena
GUAC	38.8°N, 123.6°W	15	Coast	SIO	Gualala Point
FTRC	38.5°N, 123.2°W	25	Coast	SIO	Fort Ross
B13	38.2°N, 123.3°W	0	Buoy	NDBC	
BBML	38.3°N, 123.1°W	9	Coast	UC	Bodega Bay
B26	37.7°N, 122.8°W	0	Buoy	NDBC	
B12	37.4°N, 122.7°W	0	Buoy	NDBC	
ANNP	37.1°N, 122.3°W	12	Coast	SIO	Anuo Nuevo Pres.
SCZ	36.9°N, 122.1°W	12	Profiler	WPL	Santa Cruz
B42	36.8°N, 122.4°W	0	Buoy	NDBC	
FORD	36.7°N, 121.8°W	51	Profiler	NPGS	Fort Ord
SURN	36.3°N, 121.9°W	10	Coast	SIO	Pt. Sur
NEP	36.2°N, 121.7°W	240	Visual		Nepenthe Rest.
BCRK	36.1°N, 121.6°W	60	Coast	SIO	Big Creek Res.
B28	35.7°N, 121.9°W	0	Buoy	NDBC	
PPED	35.8°N, 121.3°W	7	Coast	SIO	Pt. Piedras Blancas
DIA	35.2°N, 120.8°W	24	Sounder	PG&E	Diablo Canyon
VBG	34.6°N, 120.8°W	125	Profile	USAF	Vandenberg AFB
B51	34.5°N, 120.7°W	0	Buoy	NDBC	
PARG	34.6°N, 120.6°W	16	Coast	SBAPC	Pt. Arguello
PCON	34.4°N, 120.4°W	17	Coast	SBAPC	Pt. Conception
B54	34.3°N, 120.4°W	0	Buoy	NDBC	
GAVI	34.5°N, 120.2°W	34	Coast	SBAPC	Gaviota
ECAP	34.7°N, 120.0°W	39	Coast	SBAPC	El Capitan
B53	34.2°N, 119.8°W	0	Buoy	NDBC	

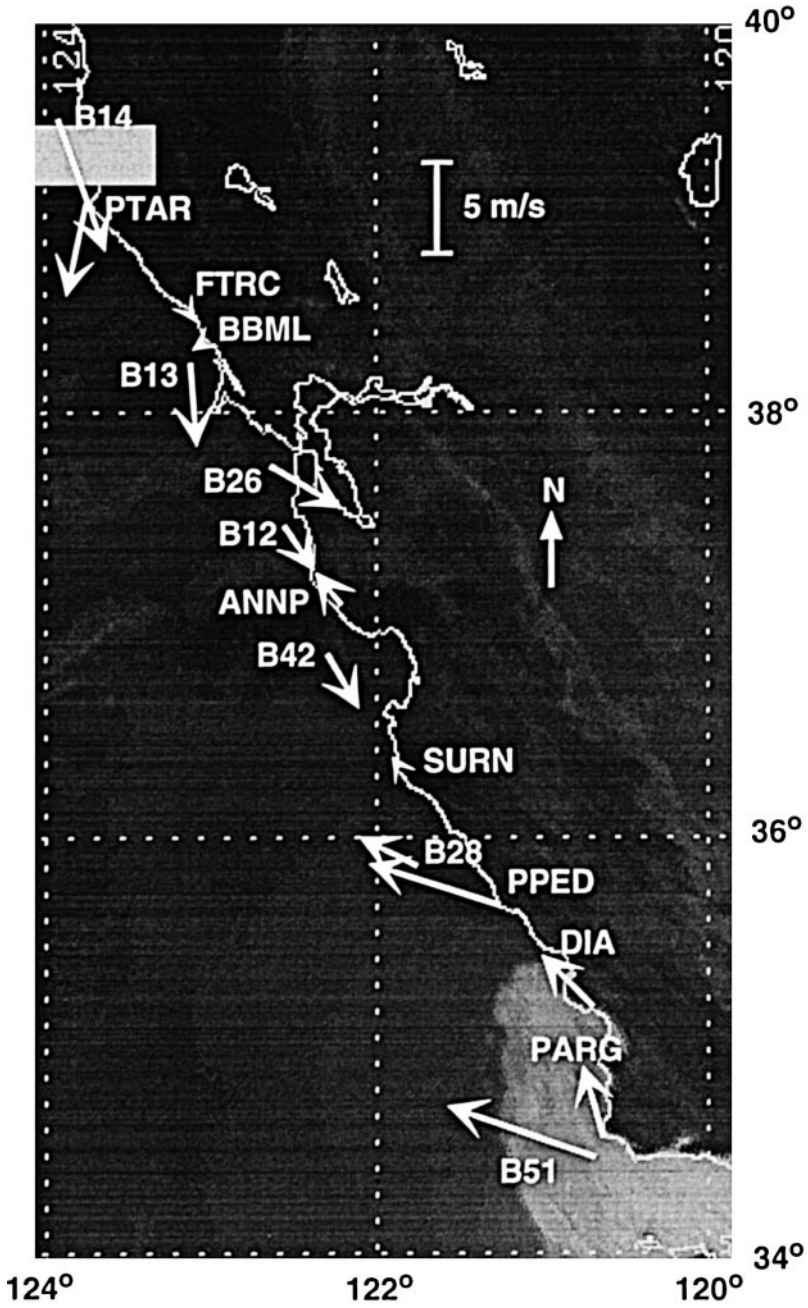

FIG. 2. The 1359 UTC 10 June 1994 visual satellite photograph. The leading edge of the stratus cloud in the SSML has just passed DIA.

aircraft was instrumented to measure winds, air temperature, humidity, pressure, and height. Vertical soundings were flown to sample the coastal atmosphere from 60 m in the clear or top of the stratus cloud, up to 1500 m.

3. The clouds and synoptic scale

On 9 June, there was a stratus overcast in the Southern California Bight while the California coast was clear. The 1214 UTC IR photo seems to show an increased obscuration which might be stratus or fog between PARG and PPED but is not shown because the contrast is too poor to be reproduced directly. Early in the morning at 1359 UTC 10 June, a stratus overcast definitely extended just to the north of PCON (Fig. 2). By 1810 UTC, the leading cloud edge over the coastal ocean had progressed considerably along the central California coast but was held back inshore at PPED (Fig. 3). By 2000 UTC, the stratus overcast offshore extended to SURN, while the cloud at the coast had extended only

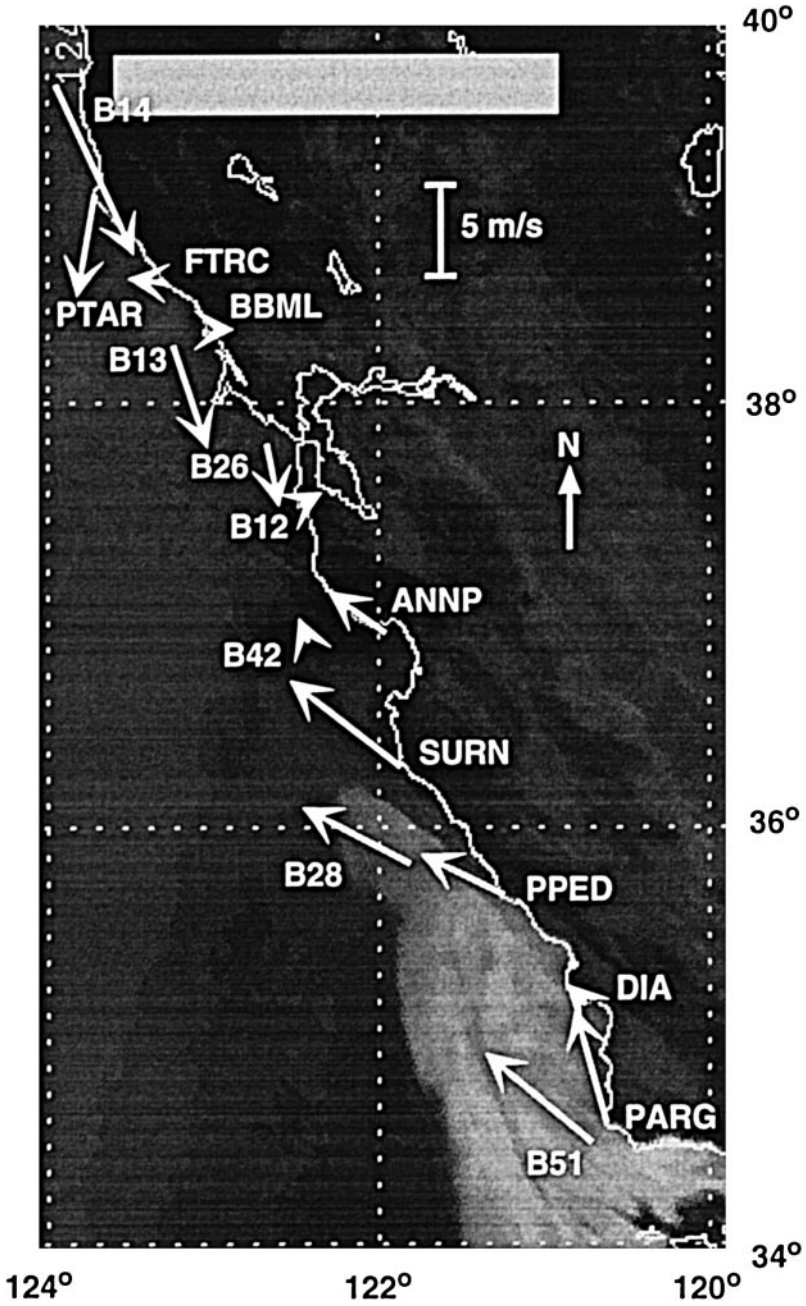

FIG. 3. The 1810 UTC 10 June 1994 visual satellite photograph. The leading edge of the stratus cloud is abreast of SURN. The colder sea surface temperature has retarded the cloud development in the coastal area just to the east.

halfway between PPED and SURN (not shown). At 2336 UTC, the next satellite photo shows the leading edge turning into Monterey Bay rather than simply progressing upcoast (not shown). After this point, the nature of the leading edge changed. It became much narrower, hugging the coast, just reaching San Francisco Bay on 11 June at about 0336 UTC (see the IR satellite picture in Fig. 4). Past this point, the progression is hard to follow, as shallow stratus clouds are hard to detect by infrared after sunset. However, the next morning's visual satellite photograph showed a cyclonic eddy in the stratus cloud adjacent to the coast and the southern side of PTAR (Fig. 5).

Along the central coast, the leading edge of the cloud at the shore was thin, low, and smooth. The structure of the leading edge was observed by two of the authors from above at the 240-m-high Nepenthe restaurant (NEP in Fig. 1) around 2300 UTC (Fig. 6). The dimensions

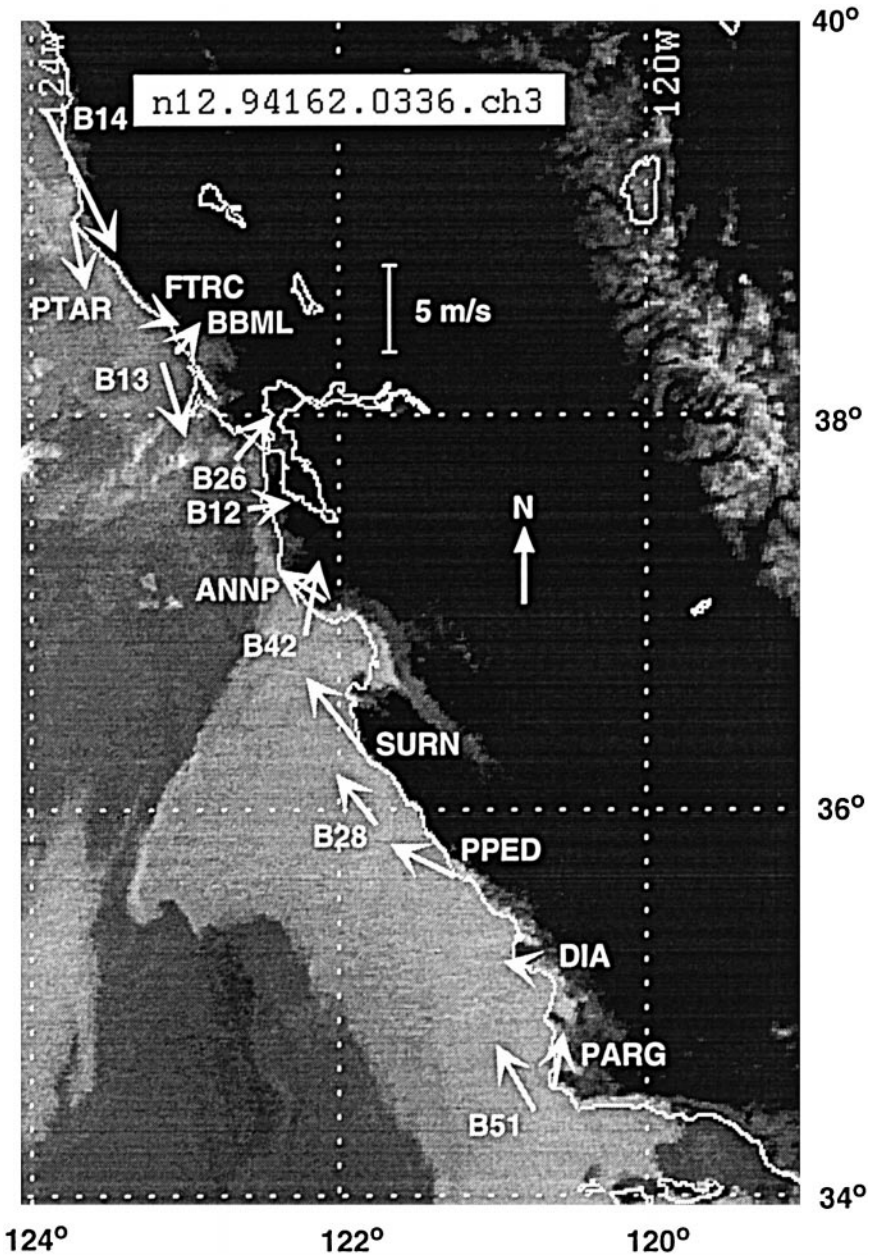

FIG. 4. The 0336 UTC 11 June 1994 infrared photograph. A wide band of stratus has reached ANNP. A narrower, 8-km-wide band of stratus extends from ANNP to the mouth of San Francisco Bay.

of the cloud were visually estimated relative to local topographic features. First to pass under NEP was a thin crest cloud perpendicular to the coast. It was about 200 m wide, had about the same base height as the main cloud, was much thinner, and maintained a constant interval of about 400 m ahead of the solid cloud edge (also seen in Fig. 6). The next to pass was the leading edge of the main cloud, which thickened rapidly at first, to about 80–120 m above sea level, then very slowly thereafter. Behind the leading edge, there are parallel cloud bands (waves) that intersect the coast that are apparent in the far left of Fig. 6. The cloud edge was recorded at the SURN station up the coast about an hour later. The alongcoast cloud structure (consisting of a rapid thickening behind the leading edge followed by slow elevation changes with a smaller, narrower cloud keeping its relative station ahead) had the distinctive structure of undular bores observed in the atmosphere (Simpson 1987) and on rivers (Tricker 1964). Later, it will be pointed out that the surface winds, pressure, and temperature structure at the nearby SURN station were also consistent with an undular bore.

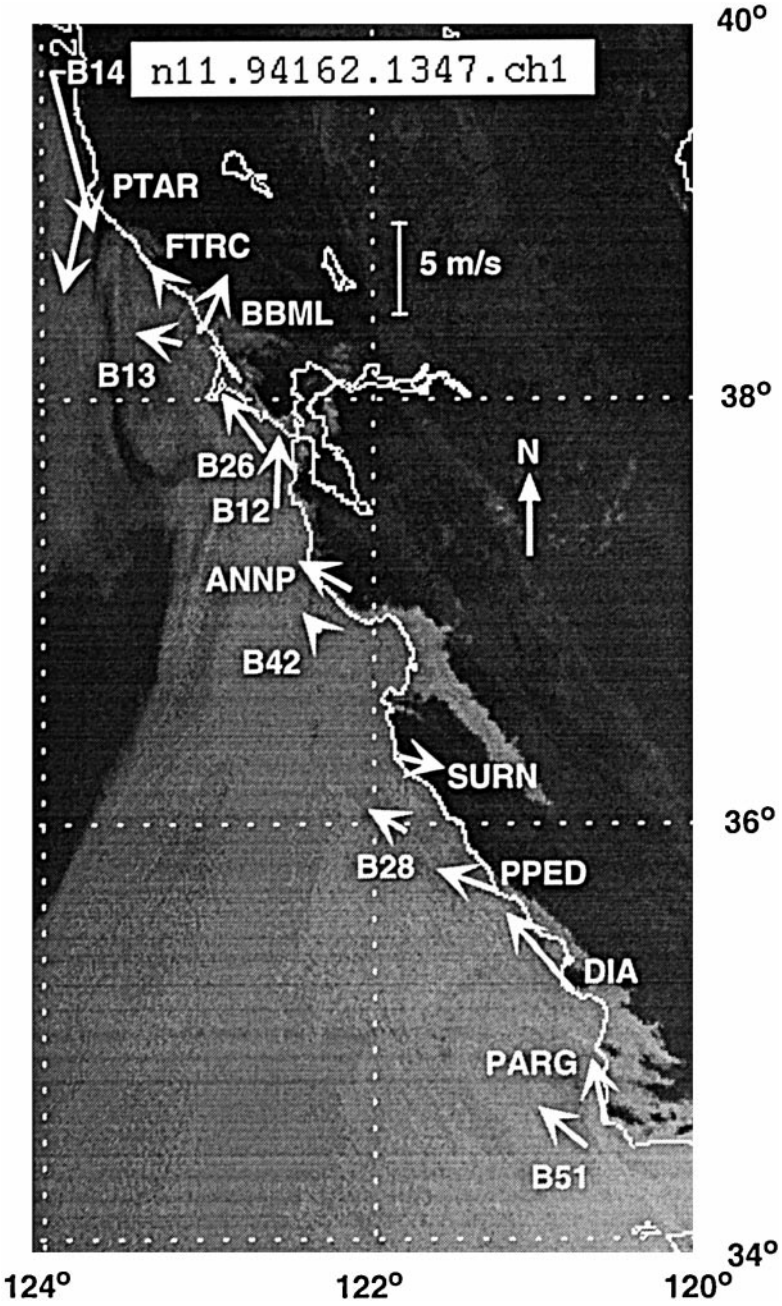

FIG. 5. The 1347 UTC 11 June 1994 visual satellite photograph. A cyclonic eddy is in the lee of Point Arena. There is a narrow separation between the stratus eddy and the stratus extending due south from PTAR and farther offshore.

Also observed to the south from the Nepenthe was the distant top of the main cloud, flat up to approximately 0.5 km of the steep coastal mountains, then rising at an angle to intersect the topography (which may have been due to shoaling at the coast). Tricker (1964) described undular river bores where the wave crest was highest at the edge of the river and ascribed this to shallower depths at the edge.

Between 2030 and 2230 UTC, when the cloud leading edge had reached Monterey Bay, the aircraft determined the cloud-top height to be 90 m at the leading edge, 180 m high some 25 km behind the leading edge, and about 165 m at a distance of 170 km behind the leading edge. Each of these measurements was made near the ''centerline'' of the cloud, approximately halfway between the coastline and the seaward edge of the cloud for-

FIG. 6. Photograph at 2300 UTC 10 June from the 246-m-high Nepenthe restaurant (NEP) taken by Dorman and Rogers while observing the cloud edge passage. View is to the southeast. The main cloud (denoted ''main bore cloud'') is the northbound, leading edge of the stratus cloud that is in the satellite photo in Fig. 3. Also noted is an advancing, isolated cloud wave crest perpendicular to the coast (denoted ''leading wave'') that maintained a constant distance before the main cloud. The structure of the main cloud leading edge and leading wave has the signature of an undular bore (Simpson 1987; Tricker 1964).

mation. At several points around the edge of the cloud formation, the aircraft observed the cloud-top height to be between 75 and 115 m.

The synoptic setting and a description of the synoptic aspects of this event are discussed in Ralph et al. (1995) and Ralph et al. (1998). An inverted trough at 700 hPa was crossing the midcoast at 1200 UTC 10 June, then moved farther east 12 h later. At sea level, a broad weak low pressure field extended northward along the California coast at 1200 UTC. After 12 h, the coastal low pressure was isolated around San Francisco. As derived from radar profilers, Ralph et al. (1995) and Ralph et al. (1998) noted there was a minimum in the boundary layer depth along the central California coast at 1200 UTC. By 0000 UTC 11 June, a coastal low had moved to the north along central California.

During the first day of the event, southerly winds appeared on 10 June first in the Southern California Bight and progressed to the north. These southerly winds extended well into California beyond the coastal mountains and up to 500 hPa, well above the marine layer (Ralph et al. 1995, 1998). It was suggested that the southerly winds were created by a midlevel feature trapped along the California coastal mountains that moved to the north. During the first day of the event, the midlevel isotherms and main subsidence inversion remained at a constant height at the coastal profiler stations at VBG, SCZ, FORD, and Fort Bragg (50 km to the north of PTAR). Thus, there was no systematic lifting of the subsidence inversion—associated with earlier cases of trapped events (Dorman 1985, 1987; Mass and Albright 1987)—during the first day.

4. Surface data

The essentials of the temporal variation of the surface coastal winds are captured in the buoys and the coastal stations. Wind direction is relative to the principal axis, which is the orientation of the maximum wind variance for that station for the entire record and positive values are winds from the south. Early on 10 June, northerly winds were seen at all buoys, between Point Arguello (B51) and Point Arena (B14) with B14, B42, and B28

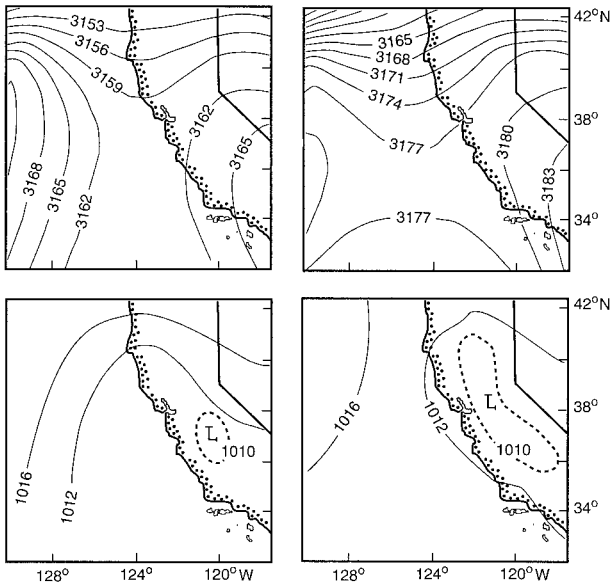

FIG. 7. National Weather Service analysis 700-hPa height (upper) and the sea level pressure analysis (lower) at 1200 UTC 10 June (left) and 0000 UTC 11 June 1994 (right). The 1200 UTC 10 June 1994 analysis corresponds to the moment when southerly winds reached the central coast. The 0000 UTC 11 June 1994 analysis corresponds to when the leading edge of the cloud was between SURN and ANNP.

particularly strong before 0600 UTC (Fig. 8a). Before sunrise, wind reversal to southerly winds began at buoys in the Santa Barbara Channel at 0800 UTC (not shown) and appear to have progressed up the coast to B13. The strength and duration of the southerly winds decreased with distance up the coast, so that only a brief reversal occurred at B13. The exception was B26 in the orderly buoy phase, with persistent weak winds probably suffering from the influence of the gap in the coastal mountains at San Francisco.

The coastal stations suggest a more complicated structure (Fig. 8b). The wind reversal began in the Santa Barbara Channel (not shown) and proceeded around PCON to PARG, leading the offshore buoys by a few hours. However, both PPED and the acoustical sounder station at DIA (not shown) lead the wind reversal at PARG by several hours. Southerly winds began simultaneously in the Santa Barbara Channel and along the open coast between DIA and PPED. In the central coast, between PARG and SURN, strong northerly winds are reversed to strong southerlies with phase progressing to the north again.

Weak winds preceded the southerly pulse at all coastal stations north of SURN and south of PTAR. The two northern coastal stations at BBML and FTRC had weak and variable winds for a day before the event. The northern limit of this event was a short slacking of northerly winds at PTAR. Thus, winds at the coast and south of PTAR to BBML were weak for the entire period despite strong northerly winds at the buoy 25 km offshore.

The nature of the leading edge of the event is revealed in the minute-averaged data from the SIO stations. The winds will be presented as the component along the principal axis (PA), which is the orientation of the maximum wind variance for that station for the entire record. The winds at all of the coastal stations used in this paper tend to align with the PA. Positive values are winds from the south.

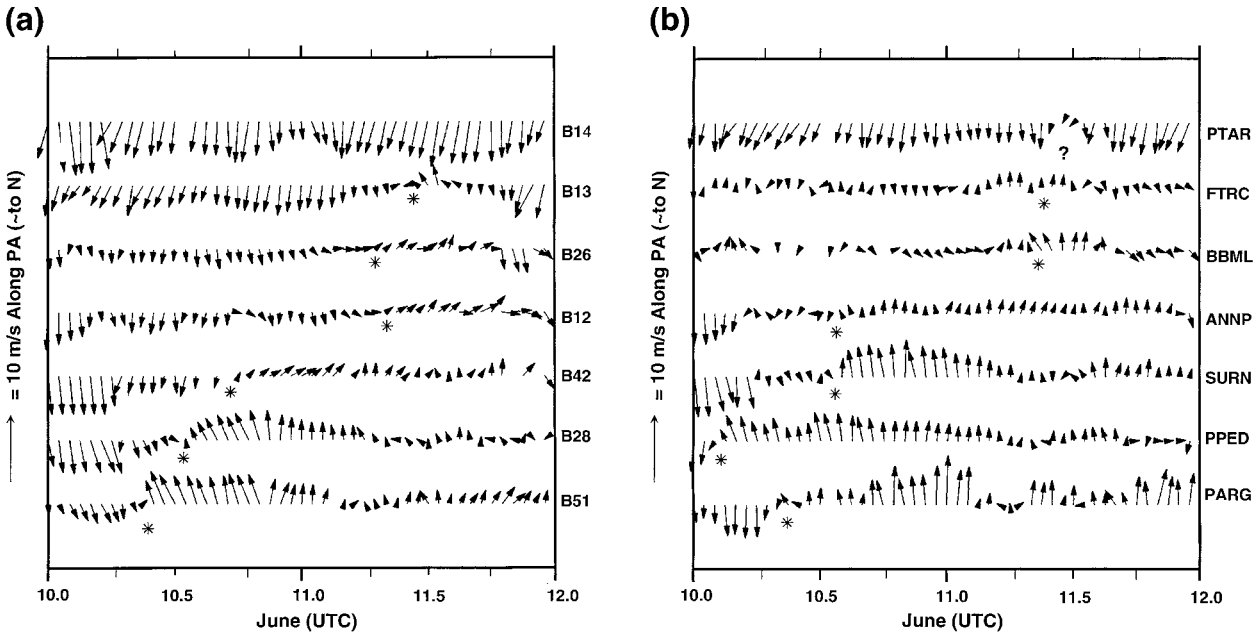

FIG. 8. (a) Buoy wind vectors. North is up. Arrows point downwind. Asterisk marks wind reversal to southerly. (b) Coastal station wind vectors. North is up. Arrows point downwind. Asterisk marks wind reversal to southerly.

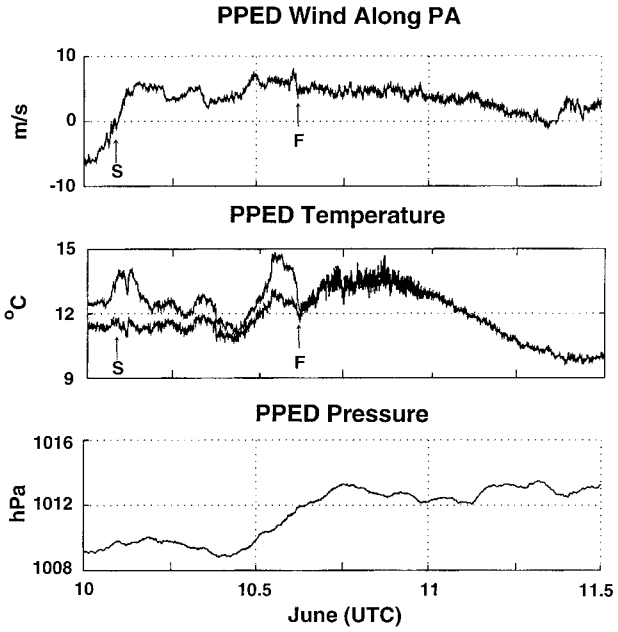

FIG. 9. PPED minute-averaged data. Winds are the component along the principal axis, which is the orientation of the maximum wind variance for that station for the entire record. Positive values are winds from the south. The upper temperature plot is the air and the lower is the dewpoint; S marks the reversal of winds to southerly; F marks saturation and fog formation.

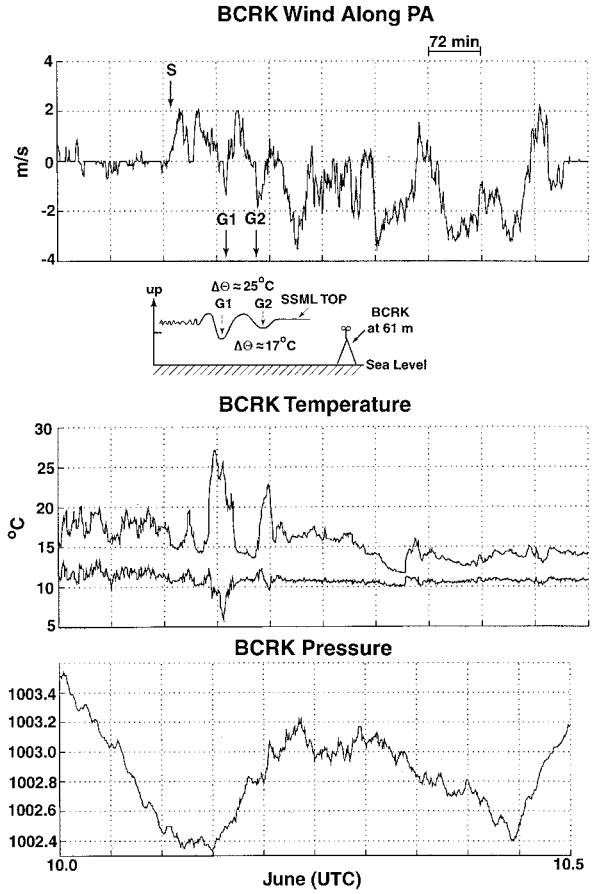

FIG. 10. BCRK minute-averaged data: S marks the reversal of winds to weak southerly. The brief large temperature increase and dewpoint decrease at G1 and G2 are believed to have been internal gravity waves that forced the air temperature inversion base below the 6-m elevation of the station temperature and moisture sensors for short periods. The cartoon shows the relation between the BCRK station and gravity waves on the top of sea surface mixed layer.

At PPED, the winds reversed smoothly from 8 m s^{-1} from the northwest to 7 m s^{-1} from the southeast (S in Fig. 9). When the wind reversed, the air temperature increased but the dewpoint remained the same. About 11 h later, the air temperature dropped to the dewpoint with the development of fog (F in Fig. 9). However, the air mass at PPED was close to saturation several days before this event.

In contrast to the other stations, BCRK had no dramatic changes during the event. The winds were weak (1–3 m s^{-1}) and variable for the first half of 10 June (Fig. 10). Around the time the leading edge of the wind shifted from northerlies to southerlies at BCRK (around 10.1–south. 10.2 in Fig. 10), there were short pulses of southerly winds of 2 m s^{-1} of marginal significance. In the first 2 h of 10 June, the air and dewpoint temperatures had higher frequency variations but values were within ranges of that associated with the sea surface mixed layer. After two short, warm events (G1 and G2 in Fig. 10), the high-frequency variations in the air temperature and dewpoint were greatly suppressed as if the station was continuously immersed in the sea surface mixed layer. Although the magnitudes were too small to accurately determine phase relationships between the variables, the variations were of a timescale of a few minutes, which would be consistent with gravity waves running along the top of the marine boundary layer (Atkinson 1981). Events G1 and G2 were of greater magnitude, so the air temperature, dewpoint, and wind speed are in phase and consistent with a solitary wave in the sea surface mixed layer. The variations at BCRK are of a structure not seen at the other coastal surface stations that are at a lower elevation. We suggest that on 10 June, the marine layer top was only the order of 10 m above the BCRK air temperature sensors that sat on top of a small, sharp cone (inset in Fig. 10). Gravity waves or other short-term variations brought the warm, dry air over the top of the layer down to the sensors, causing higher air temperatures and lower dewpoints. Upward motion of the wave would not have changed the air temperature or dewpoint as this was more uniform in the sea surface mixed layer. The hydrostatic pressure variations associated with the larger events as G1 and G2 would not have been significantly above the background noise if the top was moving only 10–20 m vertically. We shall use this later to infer that the top of the sea surface mixed layer was only about 70 m high at BCRK around this time.

Under northerly winds, the SURN station on the

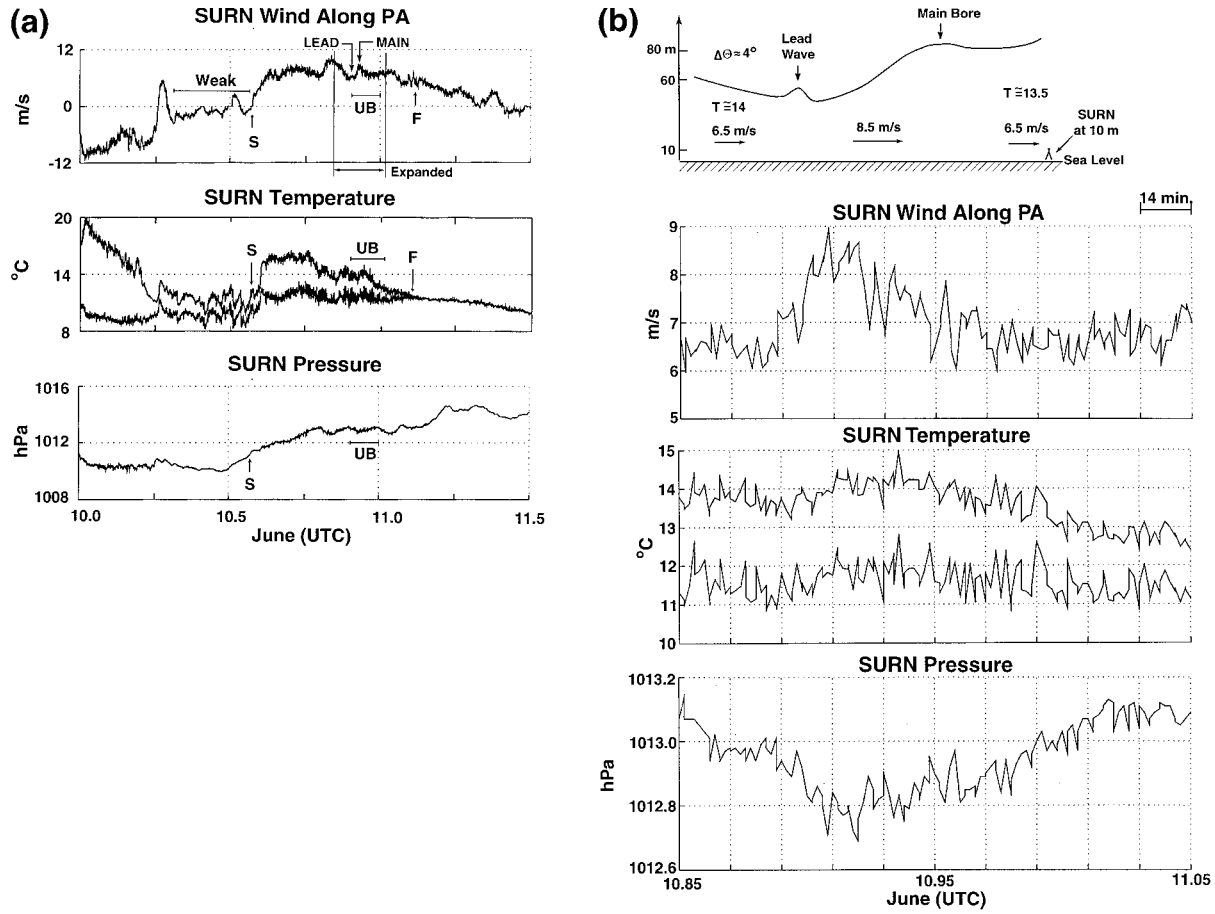

FIG. 11. (a) SURN minute-averaged data: UB notes a hypothesized undular bore. See Fig. 9 for remainder of explanation. (b) Expansion of (a) for the period of the hypothesized undular bore passage at SURN. The cartoon at the top suggests the structural changes at this station during this period.

southern edge of Monterey Bay was undergoing a cooling trend at night on 10 June. This trend was terminated by an hour-long event that brought a pulse of warmer air from the south with a small pressure rise (Fig. 11a). This was followed by weak, mostly northerly wind. Later, an abrupt shift to southeasterly winds with speeds up to 8 m s^{-1} and a temperature and dewpoint rise (S) marked the northward passage of the leading edge of the clouds.

The dewpoint switched from rising to oscillating about a mean 35 min after the southerly winds started. No significant trend was detected for the next 12 h. During the same period, the air temperature decreased to the nearly constant dewpoint temperature at which time the station was enveloped in fog (F).

The hypothesized undular bore passage, seen from NEP as noted earlier, is indicated by UB. The small increase in southerlies in Fig. 11a (''lead'') is believed to be the small crest wave leading the main cloud edge seen in Fig. 6. This is followed by the stronger southerlies believed to be associated with the main cloud edge and main bore structure (''main''). This portion, noted by ''expanded'' in Fig. 11a, is expanded in Fig. 11b where the associated air temperature increases weakly with the leading wave and more strongly with the greater changes associated with the main bore structure. The cartoon at the top of Fig. 11b suggests the relationship between the sea surface mixed-layer top, the variations, and the station near sea level at the bottom of the layer. From hydrostatics, if there was a 4°C temperature difference across the top of the sea surface mixed layer, an 8-m increase in the layer depth would cause a surface pressure change of 0.016 hPa (in the noise level), and a 20-m increase in the layer depth would cause a surface pressure rise of 0.04 hPa, which is the about the noise level. Thus, no standout pressure signal is expected with the leading of the edge of the bore. In fact, there is a small pressure rise with the leading wave and a larger pressure rise associated with the main bore edge. The structure of these variables is consistent with the signature of an undular bore (Simpson 1987).

At ANNP, strong northerly winds were followed by 8 h of weak winds, then a reversal (S in Fig. 12a) as well as increases in air and dewpoint temperature. After

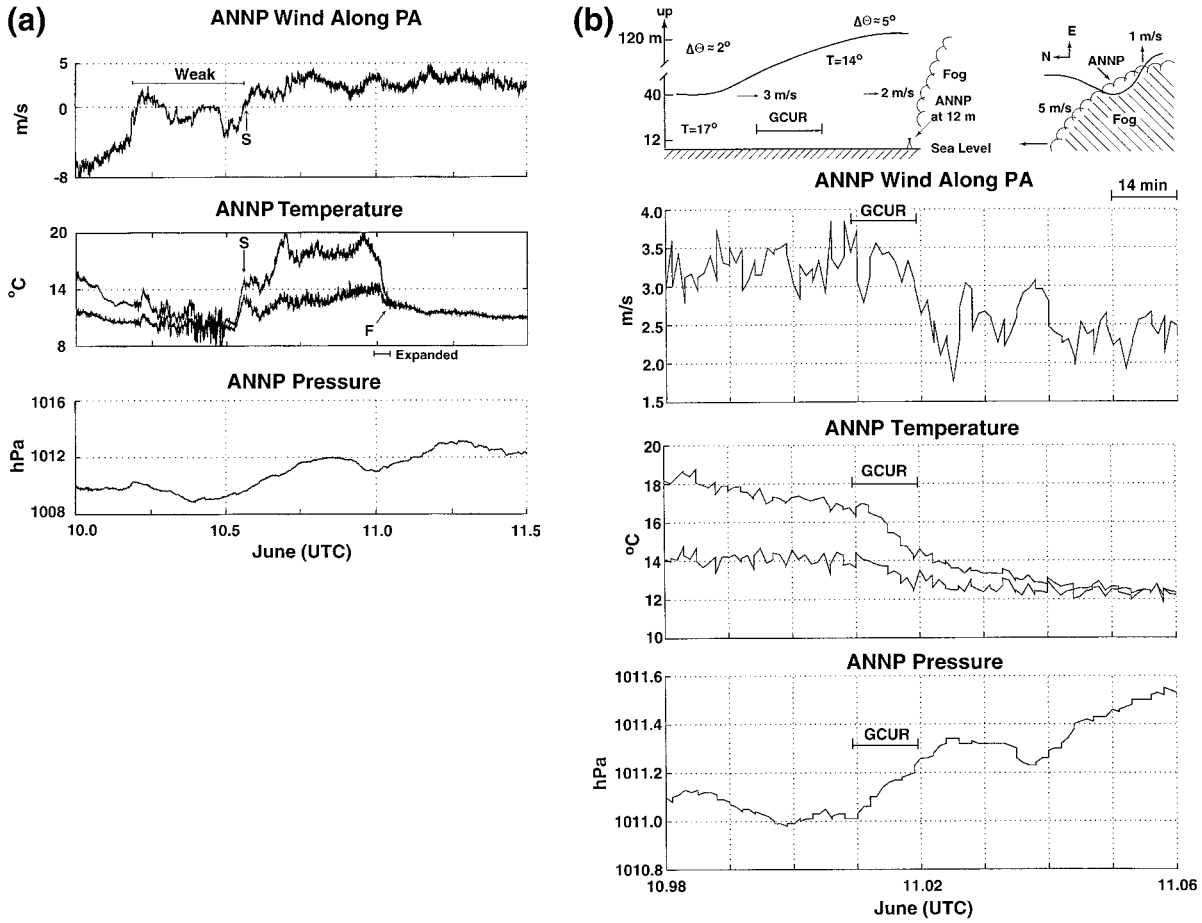

FIG. 12. (a) ANNP minute-averaged data. ''Weak'' marks weak and variable winds. See Fig. 9 for remainder of explanation. A rapid air temperature fall of 7°C in 77 min to form fog is nearly coincident with the leading cloud edge passage. (b) Expansion of the ANNP time series about the time of the sudden temperature fall and leading cloud edge passage. The steepest temperature fall is 3°C over 14.5 min and is characteristic of a gravity current. The cartoon in the upper left suggests the structural changes at this station during this period. The cartoon in the upper right is a map view of the leading cloud edge which is progressing faster alongshore than cross shore.

11 h of southerly wind and elevated air temperature, the latter abruptly fell to the dewpoint, thus causing fog. After the initial adjustment to the southerly wind onset, there was an upward trend of 2°C in the dewpoint until 0000 UTC, which suggests a modest shift in the history of the air mass. The time period of the temperature fall is is expanded in Fig. 12b. The air temperature dropped 3°C in 14.5 min. The pressure rose by 0.3 hPa, which would be consistent with an increase of 150 m of the sea surface mixed layer, assuming that the temperature difference across the top is 5°C. There was a slight increase in the southerly winds coincident with the temperature fall after 0000 UTC followed by a drop in winds to 2 m s^{-1} at the end of the pressure rise after 11.02 which could be consistant with the passage of a leading edge of a weak gravity current [Dorman (1987); Gill (1982); and others]. However, if it was a straightforward passage, the time to complete it should have been no more than a few minutes. We speculate that the leading cloud edge turned at the coast, forming a small angle with the coast and a substantially slower cross-coast advection velocity (shown in the cartoon in the upper right of Fig. 12b). The net effect would have been to greatly increase the time for the leading edge to completely pass. An offshore wind component sliding over and dragging on the denser marine layer would have reduced the cross-shore advection speed. A cross-shore advection speed one-fifth that of the along shore speed would mean the leading edge would have passed over water in about 3 min (consistent with a gravity current). In fact, this type of cloud advection was observed by two of the authors 30 km north of Point Sur, where the leading cloud edge of this event passed rapidly over the water but took much longer to edge laterally inland. On a larger scale, the overwater leading edge advecting faster than that over the coast may be seen in Fig. 3. Thus, the gravity current structure was associated with the cloud edge and surface boundary layer, not the larger-scale reversal in the alongshore wind. An alternative explanation for the changes at ANNP is that the marine

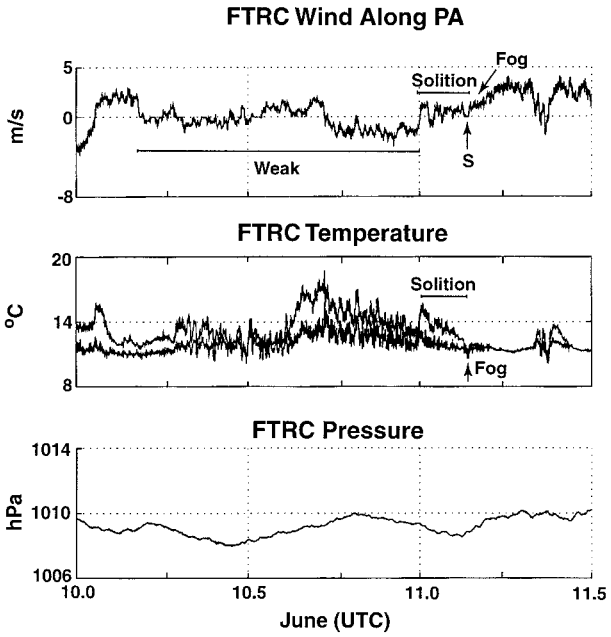

FIG. 13. FTRC minute-averaged data. ''Soliton'' marks a hypothesized soliton. See Fig. 9 for remainder of explanation.

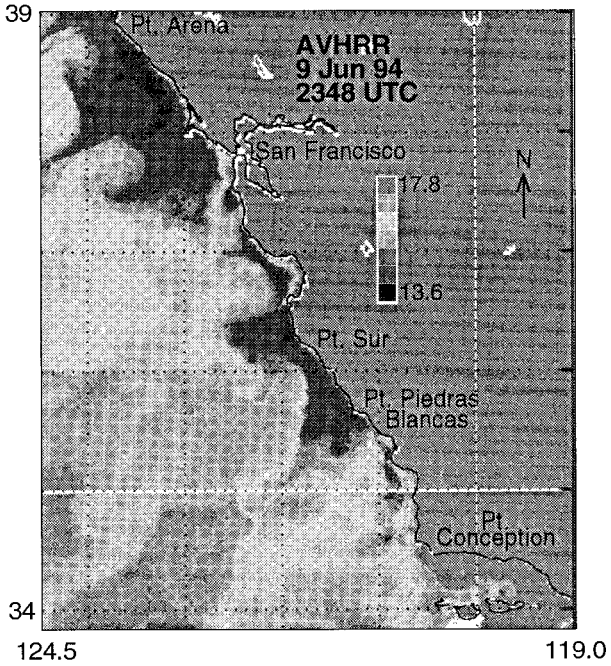

FIG. 14. Satellite AVHRR measured sea surface temperature map for 2348 UTC 9 June 1994.

layer deepened by other means, such as synoptic-scale forcing. This seems less likely as the air temperature and dewpoint should have remained about the same (which it did not) as ANNP would be bathed in local air mass. This alternative would also not have accounted for the southerly wind being correlated with the air temperature decrease.

FTRC experienced along period of weak winds and moist air (Fig. 13). This ended with an interesting event (''soliton'' in Fig. 13) consisting of four waves in wind speeds, each with a southerly and northerly phase. The waves are coincident with changes in temperature and pressure and the timescale is characteristic of gravity waves (Atkinson 1981). A train of waves, with the amplitude largest for the first wave then decreasing with each successive wave (rank ordered), is the characteristic signature of a soliton (Benjamin 1967; Christie et al. 1979). With the passage of the hypothesized soliton, the air temperature first increased and then, in the mean, decreased to the dewpoint temperature so that fog enveloped the station (F). The hypothesized soliton, associated with density intrusions in other locations, could have been on the leading edge of a weak gravity current moving northward.

5. Sea surface temperatures

The best perception of the sea surface temperature structure is obtained from the AVHRR satellite image on 9 June when the coast was cloudless (Fig. 14). It was warmest in the Southern California Bight where the earliest surge began. A warm band of water extended from the coast outward between PARG and PPED where southerly winds preceded those at PARG. The coldest temperatures were next to the central coast between PPED and SURN with much warmer water beyond 20 km offshore. Another relatively warm band was around the mouth of San Francisco Bay, and an intensely cold area existed between BBML and PTAR.

The AVHRR air temperature appears to have been systemically 1°–2°C greater than the sea temperature north of PCON under the southerly winds based upon some of the buoys and the land stations. The failure of the B28 sea temperature sensor (B28 will be discussed later) and the B42 air temperature sensor prohibits direct comparison. However, the sea–air temperature contrast was much more extreme at B26 where hot air advected from land out the San Francisco gap, causing a sea–air difference greater than 10°C.

6. Sea level pressure

Select pressure differences between representative stations are shown in Fig. 15 (a negative value means higher pressure to the south). Arrows mark time of wind reversal to southerly for each station. Along the central California coast, the buoy pressure difference at B28 and B51 and the coast pressure difference between SURN and PPED became insignificant coincident when wind direction reversed at the southern station of the pair. In this area, the coastal pressure differences are generally less than the buoy's and the reversal to southerly occurs earlier.

Offshore of the general San Francisco area, B13–B12, was negative for the whole period (which should be

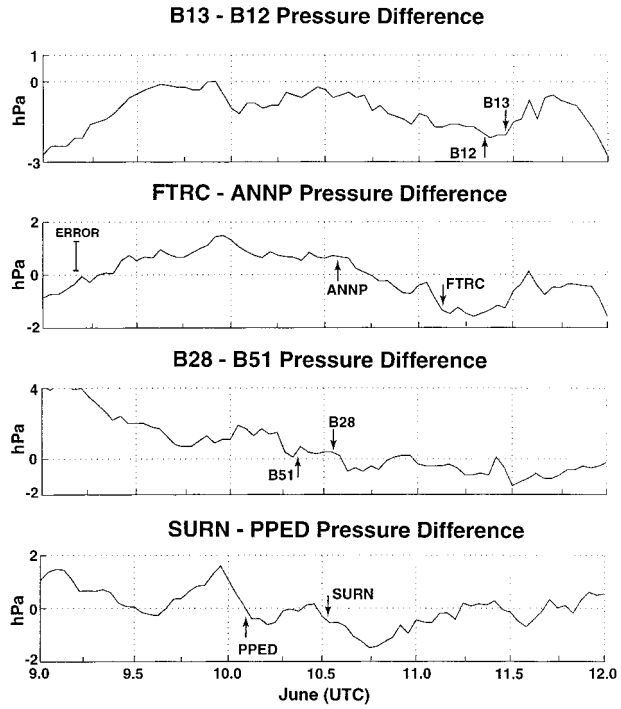

FIG. 15. Pressure differences between selected pairs of buoys and the corresponding coastal stations along the north coast (upper two frames) and the central coast (lower two frames). Arrows indicate wind shift to southerlies for station designated. Bar is possible maximum absolute error between two stations.

associated with southerly coastal winds) but had a maximum difference on the morning of 11 June when the winds at the two buoys switched to southerly. No obvious errors can account for the seemingly anomalous data as both buoys appear to be consistent with the surrounding stations. In contrast, the pressure difference at the corresponding coastal pair of FTRC–ANNP was significantly higher to the north around 0000 UTC 10 June, then switched sign when the wind reversed between ANNP and FTRC. Of the two lines, the coastal pair seems to be more in keeping with our expectation of the relationship between the winds and the alongcoast pressure difference.

Not shown is the B14–B13 difference, which was always greater than the +2 hPa that is consistent with strong northerly winds. Also not shown is the B12–B28 pressure difference, which was generally weak (less than 1 hPa) for 9–12 June, but consistently higher to the south on 10 June. The weak B12–B28 differences may reflect the complicated topography and associated flows along this coastal section.

7. Vertical structure and layer height

The unique aspect of this event is the thinness of the boundary layer that contained the stratus cloud. The best direct observations of this were made from the light aircraft. Several vertical profiles down to the cloud, but not into it, found the top to be about 150 m above sea level away from land and in the northern portion of the cloud on the afternoon of 10 June. One sounding was made down to 56 m about 10 km in front of the leading edge at 2156 UTC just to the west of the mouth of Monterey Bay, which revealed an SSML air temperature inversion of 2°C based at 140 m and a much stronger subsidence inversion based at 270 m (Fig. 16).

Three balloon soundings were taken from the ship *Glorita,* one in Monterey Bay, another one southwest of the Monterey Bay in the clear 15 km offshore, and the third in the leading edge of the cloud about 27 km offshore of SURN (positions shown in Fig. 1). The vertical sampling interval was about 30 m. Most of the boundary layer winds were missing. Launching procedures and sheltering by the ship could easily have introduced errors of a few degrees in the air temperature and dewpoint in the lowest data, although the sea level values are generally consistent with the other observations. The G2 sounding made in near-saturated conditions showed a rapid warming in the lowest 30 m, which is suspicious. A further conflict is that the balloon

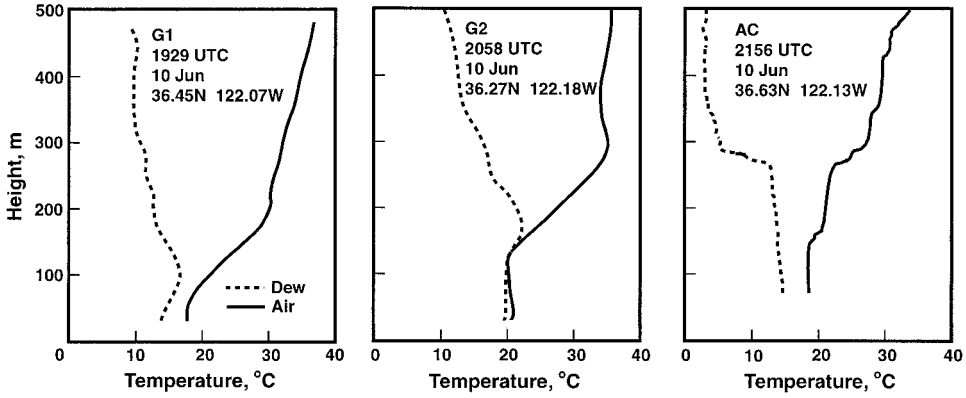

FIG. 16. The R/V *Glorita* balloon soundings at 2000 UTC (G1) in the clear and 2100 UTC (G2) through an overcast stratus of the leading cloud edge. Aircraft sounding for 2200 UTC (AC) in the clear. The arrows point to the top of the SSML and the air temperature inversion base.

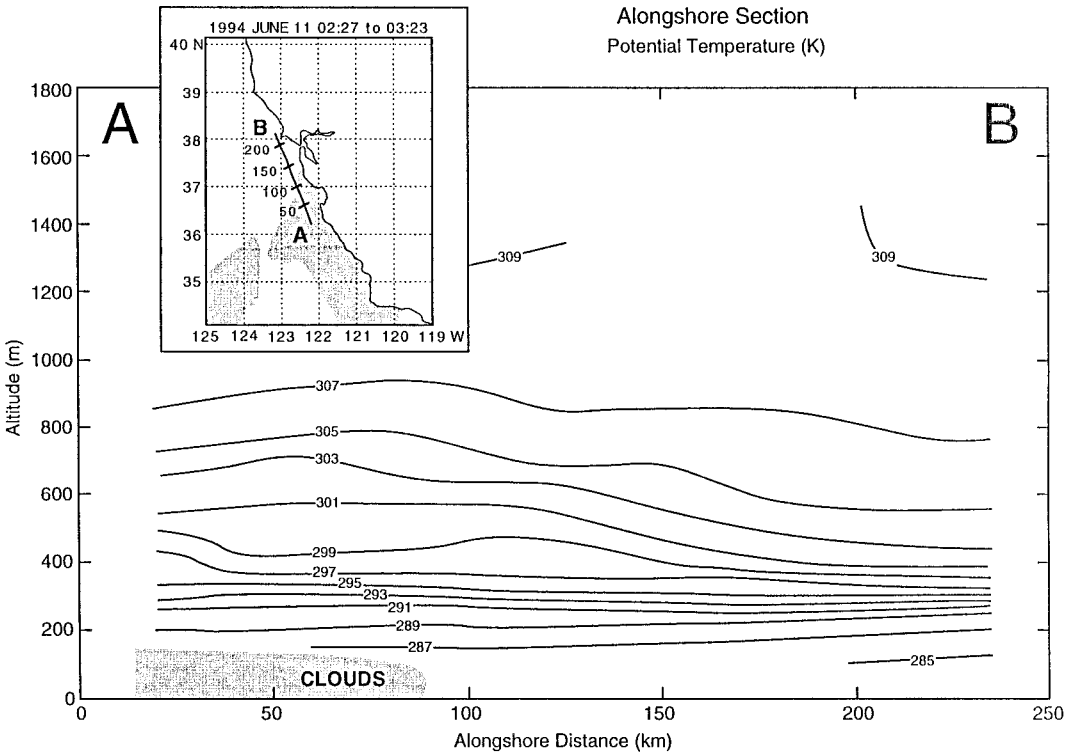

FIG. 17. Alongshore section of the potential temperature as measured by seven aircraft soundings made while flying perpendicular to the leading edge of the cloud front. View is looking west with north to the right. Shaded area is the cloud that the aircraft did not penetrate. The main subsidence air temperature inversion is 250–300 m in elevation for the entire section.

soundings were much warmer than the aircraft temperatures. Nevertheless, the relative changes required to determine the inversion height should be reliable in the balloon soundings. The air temperature inversion base was 60 m in the bay, 80 m to the west in the clear, and 140 m in the cloud (the latter two are in Fig. 16). However, the balloon sounding in the bay is not shown as it was probably more representative of the local hot offshore flow and land effects than that of the open coast.

As was noted above in the cloud section, the top of the leading edge cloud by the coast visually observed at NEP was estimated to be 80–120 m. The cloud edge was estimated to be about 64 m at BCRK (south of SURN) as this was the height of the anemometer above sea level, and no significant southerly winds were recorded at this station during the first day of this event. As noted earlier and shown in Fig. 10, there were substantial oscillations in the BCRK air temperature (7°C change in an hour) and dewpoint over this period, which suggests that the top of the boundary layer was close to the elevation of this station but was occasionally lifted above it. The oscillations were rather symmetrical, correlated with the air temperature, dewpoint, pressure, wind speed, with a negative correlation between the air temperature and the dewpoint. These characteristics and the 30–60-min timescale of the oscillations strongly suggests that the oscillations were internal gravity waves in the boundary layer (Gossard and Hooke 1975; Atkinson 1981).

A series of seven aircraft soundings along a 220-km path running approximately parallel to shore and perpendicular to the leading cloud edge showed that the main subsidence inversion was essentially at a constant elevation of 250–300 m (Fig. 17). The maintenance of the subsidence inversion at this level for the first day of the event was confirmed by the slightly inland radar profilers at VBG (base near 125 m, above the boundary layer), SCZ and FORD (boundary layer dominated by nonmarine conditions), and Fort Bragg (on the coast 100 km to the north of Point Arena). Thus, the picture emerges that during the first day of this event there was not a lifting of the subsidence inversion that caps a moist, cool marine layer as was seen in other cases of coastally trapped events (Dorman 1985, 1987; Mass and Albright 1987; Reason 1989; Reason and Steyn 1990, 1992).

8. Discussion of events

The purpose of discussion of this event is to bring together various elements having an upcoast phase progression as shown in the diagram in presented in Fig. 18. The alongcoast distances were calculated beginning

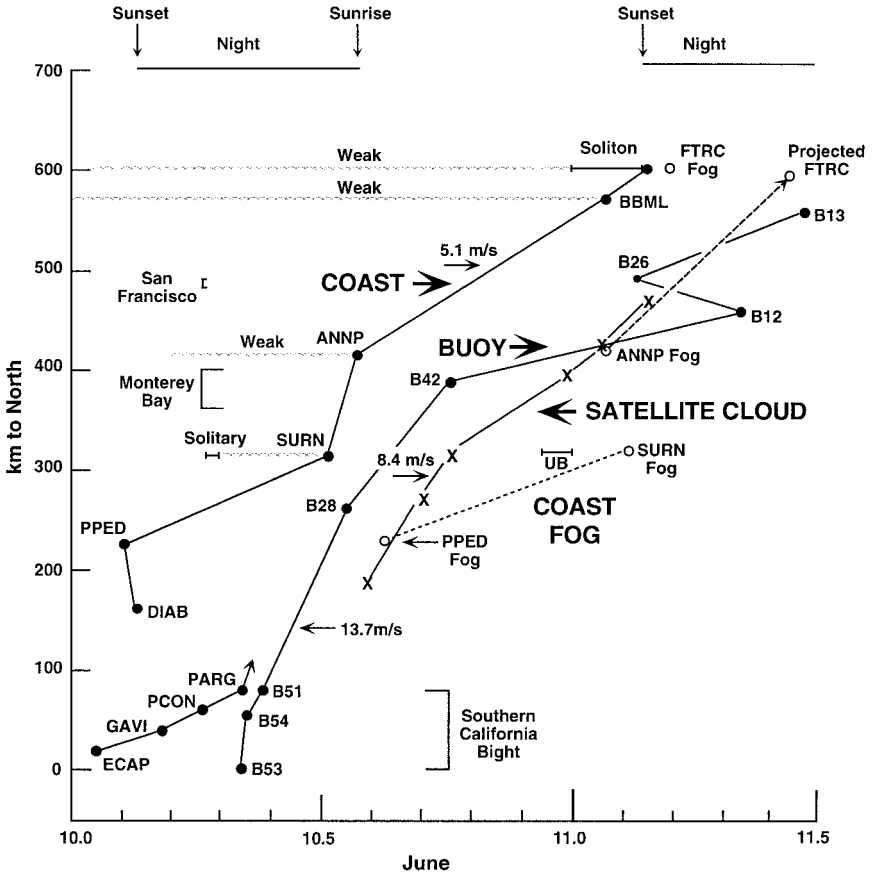

FIG. 18. Phase progression to the north relative to B53 near Santa Barbara; the initiation of the southerly winds at the coastal stations (left line) and the buoys (to the right) with station coordinate in distance and time marked with a dot. The position of the leading cloud edge is noted with an ''×.'' Numbers (m s^{-1}) is the alongcoast phase speed between the two dots (stations) or two ×'s (leading cloud edge positions). Occurrences of fog, solitary wave, and soliton are noted. Weak winds are noted by a wavy line, undular bore is designated by UB, and darkness is indicated by the line across the top of the figure.

at B53 in the Santa Barbara Channel, the site of the first reversal to southerly winds, and then essentially following the coast to Point Arena. Time is plotted across the bottom. The occurrence of the reversal to southerly winds is plotted with a solid dot and the station symbol. The coastal stations are connected with one line and the buoys with another, as the reversal always occurred at the coast first. The ''early'' reversal at DIA and PPED compared to the Santa Barbara Channel, and the fact that the phase progression between PARG and SURN is three times faster than the sea level winds suggests that southerly winds were initiated in both places simultaneously by the lower-level forcing feature discussed in Ralph et al. (1995). Selected upcoast progression speeds are posted in the Fig. 18 and in Table 2. For SURN, a wavy line designates weak northerly winds before the onset of strong southerly winds. UB indicates the changes with the signature of an undular bore at SURN discussed earlier.

TABLE 2. Selected phase speeds (m s^{-1}).

Station pair	Phase speed	Type
GAV-PARG	3.3	Coast
PARG-SURN	15.5	Coast
PPED-SURN	2.6	Coast
ANNP-BBML	5.1	Coast
B51–B28	13.7	Buoy
B28–B42	6.9	Buoy
B42–B12	1.4	Buoy
B12–B13	10.6	Buoy
185–315*	8.4	Cloud
390–465*	5.4	Cloud

* Kilometers to north alongcoast from B53.

Once started, the wind reversals divide into the central coast and north of ANNP. Along the central coast (between PPED and SURN), the coast reversals lead those at the buoys, and the buoy reversals lead the fastest satellite-estimated leading cloud edge (the estimated northernmost position is designated by an ''×'' connected by a solid line). Persistent northerly surface

winds reversed to strong southerly. The coastal fog (designated by open circles connected with a dashed line, assumed to form when the air temperature equals the dewpoint at a coastal station) occurred simultaneously with the offshore cloud edge passage at PPED. At SURN, the fog occurred 14 h after the wind reversal and 9 h after the passage of the first cloud edge. Delay of the cloud arrival and the fog at SURN may be related to the low sea surface temperatures which required longer cooling to bring the air into equilibrium with the sea surface. At ANNP, strong northerly winds are followed by 8 h of mostly weak northerly winds (designated by a wavy line) before the initiation of strong southerly winds. The time delay between first southerly winds and cloud edge passage is 12 h at ANNP followed shortly by fog formation. The lag of the cloud edge passage after the southerly wind reversal was only 4 and 6 h at B28 and B42, respectively. The fastest cloud advection speed along the central coast was 8.4 ms^{-1} which was faster than the surface 5 m s^{-1} wind speed.

North of ANNP, the character of the wind shift and phase progression changed. The reversal at B26 seems anomalous, possibly due to the effect of the San Francisco gap in the coastal mountains. The preceding winds were weak and variable at the BBML and FTRC (designated by wavy lines) for a day or more before the southerly pulse arrived, so the latter is considered the reversal occurrence in Fig. 18. The hypothesized soliton at FTRC, which is assumed to have occured just before the wind reversal, is designated by ''soliton.'' North of ANNP, the southerly winds were much weaker.

Even more significant was that the cloud edge led the reversal at the buoys. The fog formation at the coastal station ANNP (circle designated ''ANNP Fog'' in Fig. 18) occurred simultaneously with the satellite-derived cloud edge passage. The satellite-derived phase speed of the cloud edge from ANNP to San Francisco was about 5 m s^{-1}. North of this point, it was hard to definitively establish the leading edge of a southerly ''surge,'' and nightfall prevented visual tracking by satellite. Local nocturnal cooling with the hypothesized soliton initiated fog several hours earlier at FTRC, which was close to saturation before nightfall, masking any possible fog signature due to passage of a later event. However, if the satellite-derived cloud edge was extrapolated from ANNP (dashed line in Fig. 18) the surge would pass FTRC (''Projected FTRC'' in Fig. 18) and GUAC before sunrise, and arrive at PTAR around sunrise (not shown in Fig. 18) near the time that there was a brief weakening of the northerly winds (designated by the question mark in Fig. 8b). Southerly or weak flow at the coast and strong northerly flow at 25 km offshore at B14, B13, and PTAR are likely to be related to the cyclonic eddy in the cloud field observed by the early morning visual satellite photograph (Fig. 5).

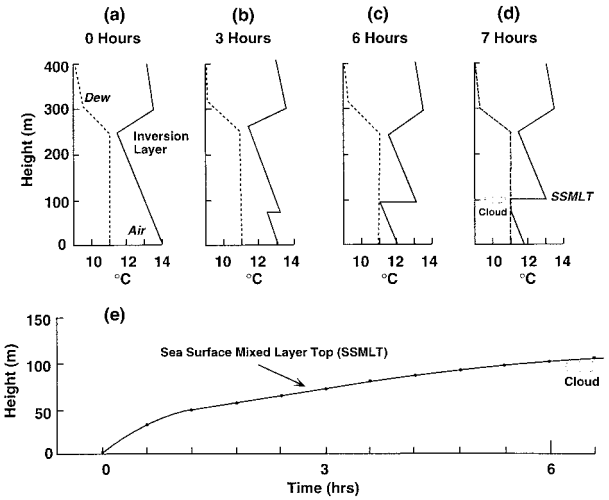

FIG. 19. Model of the SSML growth. Profiles (a)–(d) are shown for selected stages of the SSML height (e). As the SSML thickens, heat is lost to the colder ocean. A cloud forms after the air temperature at the top of the SSML equals the dewpoint.

9. Explanation

A process is needed to explain the physical events in the lower 150 m of the atmosphere. Here we divide the event into the central coast (PPED to SURN), north-central coast (ANNP to San Francisco), and the north coast (BBML to PTAR). It is proposed that the stable boundary layer (SSML) physics is key over the water along the central coast. Initially, there was a subsidence air temperature inversion near 250 m. Below, strong northerly winds and colder air moving over warmer water set up a more or less classical, well-mixed marine layer with a uniform dewpoint and an adiabatic lapse rate (Fig. 19a). With the reversal to southerly winds, warmer air began moving over colder water which formed a new SSML that began at the sea surface and grew upward by turbulent mixing. The new SSML had an adiabatic lapse rate and was neutrally stable. Across the top of the layer was a stable, stepped decrease in density. The drag of the 5 m s^{-1} southerlies on the sea surface generated frictional turbulence in the airflow, which caused entrainment of warmer potential air downward into the neutral mixed layer while heat was lost to the sea surface. Several authors have suggested that under stable conditions with heat loss to the surface, a neutral boundary layer eroding into a stable capping layer will grow proportionally to the square root of the time (Brook 1985; Stull 1983; Surridge and Swanepoel 1987). While this has been applied to only overland conditions with substantially larger cooling rates, there is no indication that they are not applicable over the sea. One formulation for the height growth (H) of the SSML is given by

$$H = \sqrt{-QBt}, \tag{1}$$

where Q is the sensible heat lost to the sea, and t is

time elapsed (Stull 1983, 1988). Parameter B is an empirically derived, site-dependent turbulence parameter that is not available for over-water conditions. Nevertheless, the growth of the SSML with time halfway between the buoys and the shore is represented in Fig. 19e. The heat loss from the air to the water is calculated from the bulk formula,

$$Q = \rho C_d C_p (T_s - T_a), \tag{2}$$

where ρ is the density of air (1.22 kg m^{-3}), C_p is the heat capacity of air (10^3 m^3 s^{-2} K^{-1}), and T_s and T_a are the temperature of the sea and air, respectively, in degrees Celsius. The drag coefficient C_d, generally assumed to be a function of stability, has been estimated between 0.66 and 1.3×10^{-3} for stable conditions [more recently reviewed in Blanc (1985) and Stull (1988)]. Used here is the intermediate value of 0.86×10^{-3}, which also was suggested by Friehe and Schmitt (1976). Using 5 m s^{-1}, and sea–air temperature difference of 2°C, the bulk heat loss from the air is about 6 W m^{-2} which would cause a 100-m-deep layer of air to cool about 2°C in 6 h. This process has been modeled in laboratory tank experiments reported in Turner (1973). Thus, as the SSML grew with time it would cool, forming a greater thermal contrast with the air immediately above, as represented in Figs. 19b,c. After 6 h, the air temperature at the top of the SSML converged with the dewpoint, forming a cloud (Figs. 19d and 19e). In theory, the cloud would grow downward, stopping when the air temperature equaled the sea temperature. In practice, the formation of the cloud would change the thermodynamics of the top of the SSML, possibly forming a subcloud layer.

The sea–air temperature difference was largest next to the coast (about 4°C). This could have caused a slower layer growth due to the greater density contrast across the top of the SSML that had to be overcome. Offshore, the sea–air temperature difference is 1°–2°C, which would allow faster growth of the SSML and earlier cloud formation. The sea–air temperature differences would explain the observed shallower SSML depths and the longer delay in cloud formation at the coastline.

The SSML growth as presented above is believed to be enhanced by ''shallow water'' wave dynamics. Consider that an SSML thickness and density to the south will be developing an ever-greater contrast with those to the north where the southerlies have had a shorter duration. When these differences are great enough, a northward-moving bore may form on the top of the SSML.

We may approximate the speed of the bore by

$$c_g = \left[gh\left(\frac{\theta_u - \theta_l}{\theta_l}\right)\right]^{1/2}, \tag{3}$$

where g is gravity, h is the SSML depth behind the leading edge, θ_l is the potential temperature of the SSML, and θ_u is the potential temperature of the air above (Gill 1982). A layer 150 m thick, and a potential temperature difference of 2 K between the SSML and the air above, would have a phase speed of 3.2 m s^{-1}. Thus, the thicker and denser SSML to the south should form a bore, moving northward along the SSML, decreasing the time for cloud formation at a particular location (Fig. 20). Lifting at the leading edge of the wave will help adiabatically cool air parcels to saturation if not already so. The sea surface wind speed of 5 m s^{-1} would add to the 3 m s^{-1} bore speed, resulting in the leading cloud edge advection speed of 8 m s^{-1}, which is what is observed along the central coast. A bore on the shallower coastal SSML would be even more nonlinear than offshore, forming the undular bore with a leading wave crest that was observed at the NEP (Fig. 6). A bore lapping upon the foot of the coast would also be thicker, which would explain the rise of the cloud upward in the few hundred meters closest to shore (Tricker 1964). Atmospheric bores moving along the marine inversion have been observed in other locations under similar circumstances, except that the others are on the main air temperature inversion at several hundred meters elevation (Clarke et al. 1981; Wakimoto and Kingsmill 1995).

To test the success of the model, the record at buoy

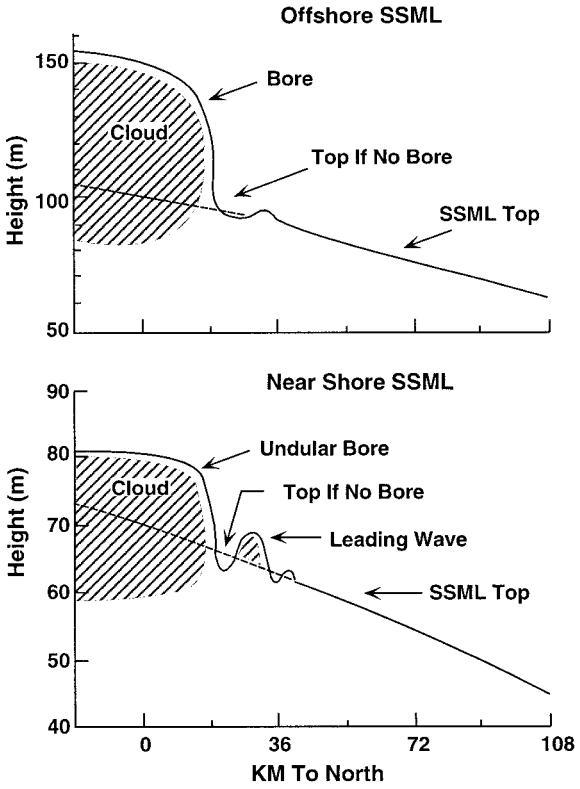

FIG. 20. Alongcoast structure of the top of the SSML with a bore moving to the right (to the north). The dashed line is the projected height of the SSML if there was no bore. The offshore condition is in the upper figure and the nearshore in the lower, which is shallower and develops into an undular bore with a separate leading wave cloud.

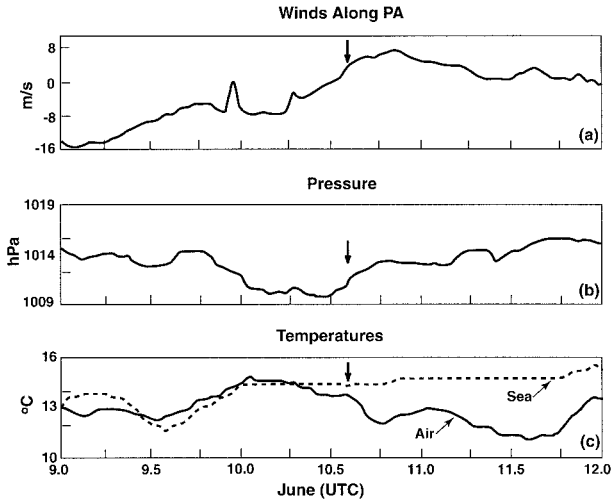

FIG. 21. Conditions at buoy 28 on 9–11 June 1994. After the wind reversal to southerlies (marked by the arrow), the air temperature only decreases, suggesting advection of adjacent cold air that was over colder seawater. The constant sea surface temperature over periods longer than 12 h may signify a failure of the sensor.

B28 was examined. The air temperature decreased monotonically beginning before the wind shift (marked by the arrow in Fig. 21) until after 1900 UTC 10 June. There was no increase in air temperature with warm air advection initiated with the wind shift, followed by a decrease as the air lost heat to the cooler sea surface such as occurred at SURN. Unfortunately, the sea surface temperature measurement, which remains suspiciously constant for more than 12 h at a time, appears to be unreliable. The satellite-derived sea surface temperature map for the day before (Fig. 14) shows that B28 was on the edge of an irregularly shaped cold water mass that was on the east and southeastern side of the buoy. A shift of the wind from northwest to southeast would have immediately advected air that was cooler than the local sea surface temperature. It appears that the conditions at this buoy had a different set of dynamics than next to the coast at SURN and so are not inconsistent with the model.

On the north-central coast, the phase progression properties and the width of the cloud change. North of ANNP the air was up to 10°C warmer than that to the south. It is proposed that when the leading edge of the bore arrived at ANNP, the dramatic contrast in the air density changed the dominating dynamics to that of a gravity current, which would have moved fastest in the region closest to shore where the density differences were the greatest. Rotation may have begun to have an effect, too, on the sudden narrowing of the cloud mass surge around ANNP. A gravity current is more consistent with the sudden drop in air temperature to the dewpoint and the nearly simultaneous arrival of the leading cloud edge at ANNP, in contrast to SURN and PPED (Dorman 1987; Reason 1989; Reason and Steyn 1990, 1992). The speed of the gravity current would be about the same as the bore (3–4 m s^{-1}) when added to the weak southerly winds in this area (2 m s^{-1}), and this would result in a cloud edge advection speed of 5–6 m s^{-1}. There does seem to be some slowing of the cloud advection to these values.

Passage of the leading cloud edge beyond the last satellite-observed point at 470 km (near San Francisco) is uncertain. We are assuming the fog formation at FTRC was due to high humidity, nightfall, and local conditions rather than passage of an SSML event. There is some indication of fog forming along this area of the coast in the 0336 satellite photograph (Fig. 4). The ''early'' southerly pulses and soliton at FTRC might be imposed from above, such as in the trapped event noted earlier. One possibility is that the cloud edge continued to advect north along the coast as a weak gravity current, which would be consistent with the soliton at FTRC that was associated with density flows in other locations. Along the coast, weak southerly flow turned cyclonically south of PTAR and then pinched off between the coastal topography and the strong northerly flow offshore at the buoys, forming the cyclonic eddy observed the next morning (Fig. 5). It is also possible that the cyclonic eddy was caused by the shear between the weak winds at the coast and the strong northerly winds just offshore.

10. Discussion and conclusions

Ralph et al. (1995) have made the case that the 10–11 June 1994 event was driven by a midlevel, northward moving feature, trapped against the California coastal mountains. This event caused the southerly winds at the sea surface along the California coast. These southerlies initiated simultaneously in the Southern California Bight and between Diablo Canyon and Piedras Blancs and progressed to the north. Observations show that an over-water SSML evolved to 80–140 m in depth after about 4–5 h. The SSML growth is accounted for by frictionally generated turbulence in a neutral, well-mixed layer capped by a stable layer in which the growth rate is proportional to the square root of the time elapsed since the wind reversal. The air temperature of the SSML is determined by the growth of the layer through heat loss from the warmer air to the colder sea surface and by the preexisting air temperature and dewpoint profiles. The layer velocity is expected to decrease with time due to friction and the deepening SSML, although the authors have no direct observations of this.

The satellite-observed stratus cloud was entirely contained in the thin SSML. Along the central California coast, the leading cloud edge advected fastest between the coast and the offshore buoys, which was about 50% faster than the SSML wind speeds. The cloud was initially formed, then the falling air temperature (with an adiabatic lapse rate) closed on the dewpoint (constant value) at the top of the SSML. The leading cloud edge had the signature of an undular bore near SURN. A

northward moving bore that formed on top of the SSML adds 3 m s^{-1} to the mean winds of 5 m s^{-1} for the observed cloud advection rate of 8 m s^{-1}. Further, this bore would have accelerated the lifting of the air, adiabatically cooling moist parcels at the top of the SSML to saturation. The longest time between southerly wind reversal was at the coast, between PPED and PSUR, where the sea–air temperature difference was greatest (4°C). It was least offshore at the buoys where the sea–air temperature difference was the least (1°–2°C). Bulk sea surface sensible heat loss from the SSML to the sea can account for the average temperature fall and depth of the layer. As a result, it would take longer for cloud formation over the colder inner coastal water and less over the offshore water. The cloud leading edge passage occurred after the wind reversals at both the coast and the offshore buoys.

North of SURN, the deep, cool, northward-moving SSML pushed over the warmer water with weaker southerly winds. The leading edge character shifted to that of a gravity current. This is consistent with the rapid drop of the air temperature at ANNP, which was nearly coincident with the leading cloud edge passage, characteristic of gravity currents. The horizontal scale of the cloud edge changed between ANNP and San Francisco into a narrower, coast-hugging band. The cloud advection speed of 5 m s^{-1} was the combination of the weak southerly winds (2 m s^{-1}) and the gravity current speed (3 m s^{-1}). This is consistent with the cloud edge arriving before the southerly winds at the offshore buoys.

If the cloud edge movement was extrapolated from San Francisco, it would arrive at FTRC around 0400 UTC. However, it is hard to detect at the required time an overt structure of a gravity current in the winds at BBML or FTRC. The northerly winds at the offshore buoy and at PTAR, much greater than the cloud advection speed, would have halted northerly progression (there were southerly winds at FTRC), turning into a cyclonic gyre which was observed in the next early morning satellite photo. Counter, high-speed winds halting northward progression would also be consistent with modeling by Skamarock et al. (1996), who found that both linear and nonlinear Kelvin waves would go around coastal points unless halted by opposing winds. While the SSML event is not a Kelvin wave, the midlevel feature driving the SSML is believed to have these properties. A similar result should occur for a gravity current in the SSML.

Our description of this event has bearing on the interpretation of satellite cloud advection patterns. Without direct sea surface wind observations, the assumption that the cloud edge is associated with the wind reversal could be quite erroneous and misleading. The coastal wind stations not normally available also can give a conflicting view of the coastal wind field compared to that of the offshore area. This offers a special challenge to forecasters dealing with the interpretation of ''southerly surges'' as derived mostly from satellite data and limited coastal buoy observations (Felsch and Whitlach 1993).

Acknowledgments. The Office of Naval Research supported this work under Contract N00014-94-1-0232. For allowing use of sites for the automated meteorological stations, we wish to thank the U.S. Coast Guard, UC Big Creek Reserve, El Sur Ranch, Ano Nuevo State Reserve, Fort Ross State Historical Park, and the Gualala Point County Regional Park.

REFERENCES

Atkinson, B. W., 1981: *Meso-scale Atmospheric Circulations.* Academic Press, 495 pp.

Bane, J. M, S. M. Haines, L. Armi, and M. H. Sessions, 1995: The California coastal marine layer: Winds and thermodynamics. University of North Carolina at Chapel Hill Tech. Rep. CMS-95-1, 289 pp. [Available from University of North Carolina at Chapel Hill, Chapel Hill, NC 27599.]

Benjamin, T. B., 1967: Internal waves of permanent form in fluids of great depth. *J. Fluid Mech.,* **29,** 559–592.

Blanc, T. V., 1985: Variation of bulk-derived surface flux, stability, and roughness results due to the use of different transfer coefficient schemes. *J. Phys. Oceanogr.,* **15,** 650–669.

Brook, R. R., 1985: Koorin nocturnal low-level jet. *Bound.-Layer Meteor.,* **32,** 133–154.

Brost, R. A., and J. C. Wyngaard, 1978: A model study of stably stratified planetary boundary layer. *J. Atmos. Sci.,* **35,** 1427–1440.

Christie, D. R., K. J. Muirhead, and A. L. Hales, 1978: On solitary waves in the atmosphere. *J. Atmos. Sci.,* **35,** 805–825.

——, ——, and ——, 1979: Intrusive density flows in the lower troposphere: A source of atmospheric solitons. *J. Geophys. Res.,* **84,** 4959–4970.

Clarke, R. H., R. K. Smith, and D. G. Reid, 1981: The morning glory of the gulf of carpentaria: An atmospheric undular bore. *Mon. Wea. Rev.,* **109,** 1726–1750.

Dorman, C. E., 1985: Evidence of Kelvin waves in California's marine layer and related eddy generation. *Mon. Wea. Rev.,* **113,** 827–839.

——, 1987: Possible role of gravity currents in northern California's coastal summer wind reversals. *J. Geophys. Res.,* **92,** 1497–1506.

——, 1988: Comments on ''Coastal southerlies and alongshore surges of the west coast of North America: Evidence of mesoscale topographically trapped response to synoptic forcing.'' *Mon. Wea. Rev.,* **116,** 2401–2406.

Eddington, L. W., J. J. O'Brien, and D. W. Stuart, 1992: Numerical simulation of topographically forced mesoscale variability in a well-mixed marine layer. *Mon. Wea. Rev.,* **120,** 2881–2896.

Felsch, P., and W. Whitlach, 1993: Stratus surge prediction along the central California coast. *Wea. Forecasting,* **8,** 204–213.

Friehe, C. A., and K. F. Schmitt, 1976: Parameterization of air–sea interface fluxes of sensible heat and moisture by the bulk aerodynamic formulas. *J. Phys. Oceanogr.,* **6,** 801–809.

Gill, A. E., 1977: Coastally trapped waves in the atmosphere. *Quart. J. Roy. Meteor. Soc.,* **103,** 431–440.

——, 1982: *Atmosphere-Ocean Dynamics.* Academic Press, 662 pp.

Gossard, E., and W. H. Hooke, 1975: *Waves in the Atmosphere, Atmospheric Infrasound and Gravity Waves—Their Generation and Propagation.* Elsevier Scientific, 456 pp.

Hamilton, G. D., 1980: NOAA data buoy office programs. *Bull. Amer. Meteor. Soc.,* **61,** 1012–1017.

Large, W. G., and S. Pond, 1981: Open ocean momentum flux measurements in moderate to strong winds. *J. Phys. Oceanogr.,* **11,** 324–481.

Mass, C. F., and M. D. Albright, 1987: Coastal southerlies and alongshore surges of the west coast of North America: Evidence of

mesoscale topographically trapped response to synoptic forcing. *Mon. Wea. Rev.,* **115,** 1707–1738.

——, and ——, 1988: Reply. *Mon. Wea. Rev.,* **116,** 2407–2410.

Neiburger, M., D. S. Johnson, and C. Chien, 1961: Studies of the structure of the atmosphere over the eastern Pacific Ocean in summer. I, The inversion over the eastern North Pacific Ocean. *Univ. Calif. Publ. Meteor.,* **1,** 1–99.

Ralph, F. M., P. J. Neiman, P. O. Persson, W. D. Neff, J. Miletta, L. Armi, and J. M. Bane, 1995: Observations of an orographically trapped disturbance along the California coast on 10–11 June 1994. *Proc. Seventh Conf. on Mountain Meteorology,* Breckenridge, CO, Amer. Meteor. Soc., 204–211.

——, L Armi, J. M. Bane, C. E. Dorman, W. D. Neff, P. J. Neiman, W. Nuss, and P. O. G. Persson, 1998: Observations and analysis of the 10–11 June 1994 coastally trapped disturbance. *Mon. Wea. Rev.,* in press.

Reason, C. J. C., 1989: Coastally trapped disturbances in the lower atmosphere. Ph.D. thesis, University of British Columbia, 214 pp. [Available from Atmospheric Science Program, University of British Columbia, Vancouver, BC V6T 1W51Z4, Canada.]

——, and D. G. Steyn, 1990: Coastally trapped disturbances in the lower atmosphere: Dynamic commonalities and geographic diversity. *Prog. Phys. Geogr.,* **14,** 178–198.

——, and ——, 1992: The dynamics of coastally trapped mesoscale ridges in the lower atmosphere. *J. Atmos. Sci.,* **49**, 1677–1692.

Rogerson, A. M., and R. M. Samelson, 1995: Synoptic forcing of coastal-trapped disturbances in the marine atmospheric boundary layer. *J. Atmos. Sci.,* **52,** 2025–2040.

Simpson, J. E., 1987: *Gravity Currents: In the Environment and the Laboratory.* Ellis Horwood Limited, 244 pp.

Skamarock, W. C., J. B. Klemp, and R. Rotunno, 1996: The diffraction of Kelvin waves and bores at coastal bends. *J. Atmos. Sci.,* **53,** 1327–1337.

Stull, R. B., 1983: Integral scales for the nocturnal boundary layer. Part 1: Empirical depth relationships. *J. Climate Appl. Meteor.,* **22,** 673–686.

——, 1988: *An Introduction to Boundary Layer Meteorology.* Kluwer Academic Publishers, 666 pp.

Surridge, A. D., and D. J. Swanepoel, 1987: On the evolution of the height and temperature difference across the nocturnal stable boundary layer. *Bound.-Layer Meteor.,* **40,** 87–98.

Tricker, R. A. R., 1964: *Bores, Breakers, Waves and Wakes.* Elsevier Publishing Co., 250 pp.

Turner, J. S., 1973: *Buoyancy Effects in Fluids.* Cambridge University Press, 367 pp.

Wakimoto, R. M., and D. E. Kingsmill, 1995: Structure of an atmospheric undular bore generated from colliding boundaries during CaPE. *Mon. Wea. Rev.,* **123,** 1374–1393.

Winant, C., C. Dorman, C. Frieze, and R. Beardsley, 1988: The marine layer off northern California: An example of supercritical channel flow. *J. Atmos. Sci.,* **45,** 3588–3605.